Evaluating the Structural Integrity of Spacecraft Aeroshell Designs under Severe Re-Entry Conditions

Fawzan Mohamed Kareem Navaz and Efstratios L. Ntantis[1]

Aerospace Department, Amity University Dubai, Dubai, UAE

Abstract. The structural performance of re-entry aeroshells is crucial to spacecraft mission success and safety, as they must endure extreme aerodynamic, thermal, and mechanical loads during atmospheric re-entry. This paper presents a comparative structural analysis of aeroshell nose designs inspired by Orion spacecraft capsules, evaluating flat, pointed, and hemispherical geometries under realistic severe re-entry conditions at an altitude of 60 km in the upper atmosphere. Finite element simulations incorporating steel, aluminum alloy, and epoxy-carbon-wound prepreg evaluate deformation, stress, and strain distributions using realistic material properties. The findings highlight key aerodynamic and structural trade-offs: flat-nosed designs generate higher drag but experience increased structural stress; pointed geometries offer superior aerodynamic efficiency but are prone to localized stress concentrations; and hemispherical designs achieve a balance between drag reduction and improved stress distribution. Critical stress zones and potential failure points are identified, providing insights into the limitations and advantages of each configuration. This research advances aeroshell optimization techniques to enhance spacecraft survivability during atmospheric re-entry, contributing to the development of more robust aerospace systems for future missions.

1 Introduction

Atmospheric reentry is one of the most critical and challenging phases in a spacecraft's lifecycle. During this phase, the aeroshell faces extreme conditions, including high velocity, intense aerodynamic heating, and dynamic mechanical loads. The selection of aeroshell geometry is crucial in mitigating these challenges, as it influences aerodynamic drag, heat dissipation, and structural stresses experienced by the vehicle. Among various nose geometries, flat, pointed, and hemispherical geometries have been studied for their distinct advantages and trade-offs under reentry conditions. Hemispherical nose designs, often associated with blunt-body configurations, are well-regarded for generating high drag, reducing reentry speed, and limiting heat transfer to the spacecraft. This aligns with the heat sink principle highlighted during the Apollo missions, where blunt designs effectively managed thermal loads [1,2]. In contrast, pointed geometries feature streamlined profiles that minimize drag and heating but induce higher stress concentrations, potentially compromising structural integrity during deceleration [3]. Flat-nose designs, while less common, offer a unique balance between drag and aerodynamic stability and are used in hypersonic vehicles [4]. Finite element analysis (FEA) has become an indispensable tool for assessing the structural response of aeroshells under such extreme conditions. By simulating deformation, stress, and strain distributions, FEA enables engineers to predict performance under the high-magnitude forces encountered during re-entry [5]. Material selection is equally critical; for example, advanced composites such as epoxy-carbon woven prepreg provide superior stiffness and heat resistance compared to traditional aluminum alloys [6,7].

The current paper employs ANSYS Workbench to analyze the structural performance of aeroshells inspired by Orion spacecraft capsules with different nose geometries (flat, pointed, and hemispherical) under very high-altitude atmospheric reentry conditions. The study also investigates the designs using various materials (structural steel, aluminum alloy, and composite epoxy carbon woven prepreg) to assess their deformation behavior, stress distribution, and strain patterns. By comparing these designs, the paper aims to provide valuable insights into optimizing aeroshell geometries for improved safety, efficiency, and survivability during atmospheric reentry.

2 Literature Review

Extensive research has been conducted on the design of aeroshells for reentry vehicles, focusing on nose geometries and their influence on aerodynamic and structural performance. Early studies, such as those by Allen and Eggers in [8], introduced the concept of blunt-body configurations and demonstrated their ability to dissipate heat more effectively by

[1] Corresponding author: entantis@amityunivesity.ae

creating a strong bow shock ahead of the vehicle. This principle laid the foundation for hemispherical designs used in many space missions, including the Mercury and Apollo programs [9]. Blunt designs, such as hemispherical noses, maximize aerodynamic drag, enabling adequate deceleration during reentry. However, the associated high-pressure gradients and thermal loads necessitate the use of advanced materials and thermal protection systems (TPS) [10]. Research by Braun and Manning [11] highlighted trade-offs between drag efficiency and structural stress in blunt geometries, advocating the use of improved composite materials to address these challenges. Conversely, pointed nose designs reduce drag and heat flux by promoting smoother airflow, but they exhibit higher stress concentrations at the nose tip due to localized aerodynamic forces. Schetz et al. [12] explored this trade-off and highlighted the need for precise stress management strategies, particularly for hypersonic and supersonic vehicles. Advanced materials, such as ceramic-matrix composites (CMCs), have been proposed to withstand these conditions [13]. Flat-nose geometries have received less attention in the literature but are notable for their ability to combine aerodynamic drag and stability. Studies by Bond et al. [14] revealed that flat noses are advantageous for specific hypersonic applications where high drag and stability are critical.

These configurations, however, suffer from non-uniform stress distributions and require careful material selection to avoid failure during reentry. FEA has played a transformative role in understanding aeroshell performance. Blanchard and Austin [15] illustrated the importance of high-fidelity simulations in predicting deformation, stress, and strain distributions under reentry conditions. FEA enables engineers to evaluate material behavior under extreme forces, as demonstrated in studies by Ahmed and Sharma [16], which compared aluminum alloys and composite materials for structural integrity and heat resistance. Adopting advanced materials, including epoxy carbon woven prepreg, has further advanced the field. These composites, with their superior stiffness and thermal resistance, offer significant advantages over traditional metals like aluminum [17]. Yoshida and Matsuo [18] conducted detailed studies on the strain behavior of these materials, emphasizing their role in enhancing structural integrity under high loads.

3 Methodology

Advanced FEA techniques are used to evaluate the structural performance of aeroshell cones modeled after the Orion spacecraft capsules, with flat, pointed, and hemispherical nose geometries, under re-entry conditions in the upper atmosphere. The Orion spacecraft was selected due to its advanced capabilities as a deep-space exploration vehicle, developed by NASA to carry astronauts beyond low Earth orbit. Designed for missions to the Moon, Mars, and beyond, the Orion capsule serves as the crewed module, equipped with state-of-the-art life-support systems, communication systems, and safety features for long-duration space travel. As a critical component of NASA's Artemis program, Orion plays a pivotal role in the effort to return humans to the Moon and establish a sustainable presence there. The study proceeded with selecting suitable materials, developing geometric models, setting up simulations, and analyzing the results through post-processing. This comprehensive approach provided detailed insights into the behavior of different nose configurations, enabling the assessment of their effectiveness and suitability for atmospheric reentry applications.

3.1 Material Selection

The selection of materials for aerospace applications, particularly aeroshells, is crucial due to the extreme conditions encountered during atmospheric reentry. Some of the most critical engineering materials include steel, aluminum, and composite materials, specifically structural steel, aluminum alloy, and epoxy carbon woven prepreg.

Structural steel is a highly durable material known for its exceptional rigidity, strength, and load-bearing capacity. Its resistance to deformation and high mechanical strength make it suitable for applications requiring structural integrity under extreme conditions. Although heavier than other materials, its reliability and affordability make it a common choice for aerospace structures that are not critical to weight. Structural steel is particularly advantageous in scenarios demanding high resistance to stress and strain, making it a valuable option for specific components in atmospheric re-entry and other high-stress environments.

Aluminum alloy, with its excellent strength-to-weight ratio and high thermal conductivity, is widely used in aerospace applications. Its lightweight properties and durability make it an ideal choice for components exposed to high temperatures and mechanical loads, ensuring performance and efficiency in demanding environments like atmospheric re-entry.

Epoxy carbon woven prepreg is a composite material offering exceptional stiffness, high tensile strength, and excellent thermal resistance. Its high stiffness is ideal for high-stress environments, ensuring durability and performance in demanding aerospace applications, including re-entry scenarios requiring lightweight, strong, and heat-resistant materials. The mechanical properties of these materials, shown in Table 1, were derived from established databases and literature [15,17,18].

Table 1 compares all three materials based on their mechanical properties: Young's Modulus, Poisson's ratio, density, and ultimate tensile strength.

Table 1: Material properties of aerospace materials

Material Property	**Structural Steel**	**Aluminium Alloy**	**Epoxy Carbon Woven Prepreg**
Young's Modulus *(GPa)*	200	70	395
Poisson Ratio	0.30	0.33	0.25
Density (kg/m^3)	7850	2700	1600
Ultimate Tensile Strength *(MPa)*	550	310	1200

Young's modulus, which indicates a material's stiffness, varies significantly among the three materials. Epoxy carbon woven prepreg (395 GPa) is the stiffest, followed by structural steel (200 GPa) and aluminum alloy (70 GPa). The high stiffness of epoxy-carbon composite makes it ideal for aeroshells, which require lightweight yet rigid structures to withstand the extreme aerodynamic loads encountered during atmospheric reentry.

The Poisson ratio reflects the material's tendency to expand or contract laterally when stretched or compressed. Aluminum alloy (0.33) has the highest Poisson ratio, suggesting more significant lateral deformation under stress, while structural steel (0.30) and epoxy carbon woven prepreg (0.25) exhibit the lowest values. A low Poisson's ratio enhances the durability and performance of the aeroshell nose, making epoxy-carbon woven prepreg the optimal choice for reentry applications.

A lower density is desirable for aerospace applications to minimize weight. Epoxy carbon woven prepreg (1600 kg/m^3) is the lightest material, making it highly advantageous for weight-sensitive applications. Aluminum Alloy (2700 kg/m^3) is significantly denser but still much lighter than structural steel (7850 kg/m^3), which is the heaviest and least suitable for aerospace applications where weight reduction is critical.

The ability to withstand tensile stress before failure is crucial for structural integrity. Epoxy carbon woven prepreg (1200 MPa) has the highest ultimate tensile strength, making it an excellent choice for high-performance applications. Structural steel (550 MPa) is moderately intense, while aluminum alloy (310 MPa) has the lowest tensile strength among the three. Among the materials considered, epoxy carbon woven prepreg is the most suitable choice for aeroshells due to its high stiffness, superior strength, and low density. These properties make it ideal for aerospace applications where structural performance and weight reduction are critical. Its high stiffness ensures the aeroshell maintains its aerodynamic shape under extreme reentry conditions, while its lightweight nature enhances fuel efficiency and payload capacity. Although aluminum alloys balance weight and strength, they lack the stiffness and ultimate tensile strength required for optimal performance in high-stress environments. Meanwhile, structural steel is excessively heavy despite its strength, making it impractical for weight-sensitive aerospace applications. Therefore, epoxy carbon woven prepreg is optimal for reentry aeroshells, ensuring durability, efficiency, and structural integrity.

3.2 Geometric Modelling

The selected aerospace materials are modeled as isotropic (aluminum alloy and structural steel) and orthotropic (epoxy carbon woven prepreg) to capture their distinct mechanical behavior under different loading conditions accurately. Isotropic materials, such as aluminum alloy and structural steel, exhibit uniform properties in all directions. At the same time, the orthotropic nature of epoxy carbon woven prepreg reflects its directional dependence on stiffness and strength. This approach ensures that finite element simulations provide realistic and precise predictions of material responses during re-entry, accounting for variations in stress, strain, and deformation across different material types. The aeroshell geometries are designed to reflect a conceptual design inspired by Orion Spacecraft capsules. Each nose geometry, as shown in Figure 1, is modeled with a base diameter of 5.029 meters, a cross-sectional area of 19.63 m^2, and varying nose profiles.

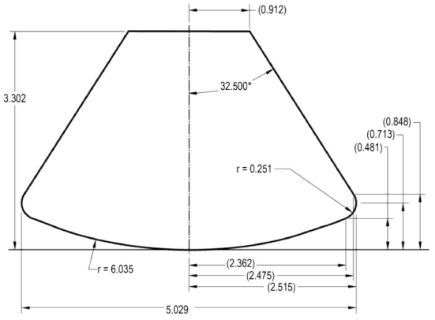

Fig.1. Vertical Cross Section of the Orion Crew Module. All measurements in meters unless otherwise noted. [19]

This paper uses three nose geometries to evaluate aerodynamic performance under reentry conditions.

The first geometry analyzed is a flat-nose design (see Fig. 2), often favored for its simplicity and straightforward aerodynamic characteristics. This flat nose features a small radius of 0.951 m and a large radius of 2.5145 m. The flat plate is 2.454 m long, providing a relatively substantial surface area for the airflow to interact with. The frontal cross-sectional area of the flat nose geometry is 2.8425 m². The flat-nose design is typically chosen for its ease of manufacturing and its ability to withstand high-pressure gradients without excessive drag. The flat-nose shape is effective at providing stability in many cases, but often sacrifices speed and fuel efficiency in high-performance scenarios.

The second geometry analyzed is the hemispherical nose (*see* Fig.3), known for its smooth, rounded shape that balances aerodynamic efficiency and structural integrity. The hemispherical nose design has a radius of curvature of 2.5145 m, equal to the base radius, resulting in a uniform, symmetrical shape. The hemisphere's curvature is 0.831 m, which plays a crucial role in how air flows around the object. The horizontal length of the hemispherical nose is also 2.454 m. This hemispherical shape is typically used in applications where stability is a key factor, as it reduces the intensity of shock waves and provides a smoother airflow transition. The rounded profile is particularly beneficial for subsonic and transonic flight regimes, where controlling drag and lift efficiently is essential for maintaining optimal performance. Furthermore, the hemispherical nose often results in a more even pressure distribution across the surface, reducing aerodynamic drag and improving fuel efficiency and overall performance, making it advantageous. The shape also reduces the likelihood of flow separation and enhances the vehicle's handling and stability under various flight conditions.

The third geometry analyzed is a pointed nose (*see* Fig.4), often used for high-speed applications due to its aerodynamic advantages. This pointed nose has a conical tip inclined at 32.5° to the horizontal, optimizing the nose shape to reduce drag by creating a more focused, streamlined profile. The horizontal length of the pointed nose is also 2.454 m, providing a consistent measure for comparison with the flat and pointed nose designs, but the key difference lies in its shape and the sharpness of the cone. The large radius of the pointed nose is 2.5145 m, and its sharp tip minimizes drag, allowing smoother airflow around the vehicle or structure. Its conical shape enhances airflow transition from the front of the object, significantly reducing the formation of turbulent wake zones that contribute to drag.

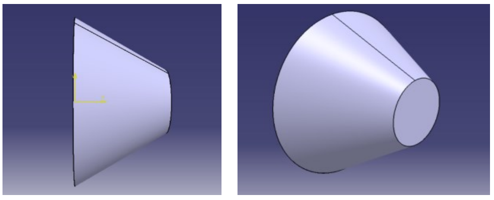

Fig.2. Flat Nose Geometry

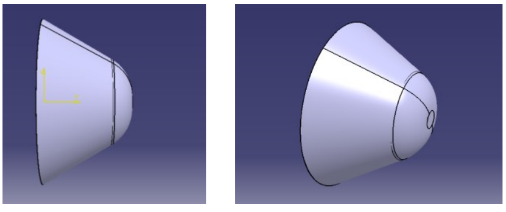

Fig.3. Hemispherical Nose Geometry

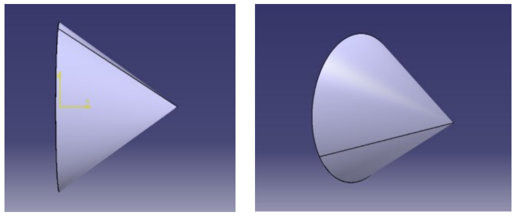

Fig.4. Pointed Nose Geometry

Figures 2-4 show the referred geometries modeled using CATIA V5 to ensure accuracy and fidelity. These models were then imported into ANSYS Workbench for meshing and analysis. Special attention was given to critical areas such as the nose tip and lateral surfaces, which are defined as named selections to streamline the application of boundary conditions. This setup enabled precise simulation of aerodynamic forces, allowing detailed comparisons of the geometries and their suitability for reentry scenarios.

3.3 Finite Element Analysis

The FEA simulations were conducted using ANSYS Workbench. A high-density tetrahedral mesh was generated to capture intricate stress and strain gradients across the aeroshell, ensuring high accuracy. A mesh independence study was performed by progressively refining the mesh until subsequent iterations showed negligible variations, ensuring numerical stability and reliability. The estimated drag force for a 5.029-meter-diameter aeroshell under high-altitude reentry conditions is approximately 10.64 MN. This force magnitude was derived using the drag force equation, which accounts for key parameters such as upper atmospheric density, reentry velocity at Mach 25, the drag coefficient for blunt bodies like aeroshells, and the frontal area of an Orion-like capsule exposed to airflow. Eq. 1 provides a systematic approach to accurately estimating the aerodynamic loads encountered during reentry. The calculated drag force was verified for consistency before being applied in the simulation, ensuring it aligned with realistic reentry conditions.

$$F_D = \frac{1}{2}\rho v^2 C_d A = \frac{1}{2}(0.01)(8500^2)(1.5)(19.63) = 10{,}639{,}690.74\ N = 10.64\ MN \qquad (1)$$

Where:

F_D : Drag Force (N)
$\rho \approx 0.01 \frac{kg}{m^3}$: Upper atmosphere (~60 km altitude) density

$v = 8500 \frac{m}{s}$: Reentry velocity for Mach 25
$C_D = 1.5$: Drag coefficient, typically 1.0 - 2.0 for blunt bodies like aeroshells
$A = 19.63\ m^2$: Frontal Area for base diameter of 5.029 m

4 Structural Analysis of Nose Geometries

The analysis primarily focused on evaluating the structural behavior of various aeroshell nose geometries under aerodynamic forces during re-entry. To simulate the attachment to the spacecraft structure, fixed supports were applied to the rear base of the aeroshell. The analysis focused on assessing the structural behavior of the nose geometries under aerodynamic forces. A static structural analysis assessed stress, strain, and deformation distributions for each geometry, providing valuable insights into its structural integrity. Reentry conditions also subject the aeroshell to extreme heat loads from atmospheric friction, altering material properties and affecting overall structural performance. Although thermal analysis is not part of this study, its significance is recognized and will be addressed in future work to assess heat flux, temperature gradients, and thermal stresses.

5 Evaluation Criteria for Nose Geometries

The performance of each nose geometry was evaluated against four critical criteria to ensure structural integrity and suitability for reentry conditions.

- Total Deformation:

Maximum displacement was analyzed to determine the geometry's ability to maintain its shape and functionality under extreme aerodynamic loading. This is crucial to ensuring the aeroshell withstands drag forces without compromising its structure.

- Von Mises Stress:

An equivalent stress measure was calculated to assess regions where the material may yield or fail. This provided insights into the structural resilience and load distribution, highlighting areas that might require reinforcement or redesign.

- Strain Distribution:

The spatial variation of strain was evaluated to identify zones of elongation and compression. Understanding these regions is essential for detecting potential deformation-prone areas that could lead to material fatigue or failure over time.

- Stress Concentration Zones

Critical regions with peak stress were identified, highlighting areas at risk of material failure and guiding design improvements to mitigate high-stress vulnerabilities.

The total deformation was assessed to determine the maximum displacement experienced by the structure under drag forces, ensuring that the geometry maintains its shape and functionality under extreme aerodynamic conditions. Von Mises Stress was used to calculate equivalent stress to identify regions where material failure could occur, providing insights into structural resilience and load distribution. Strain distribution was evaluated to understand how strain varies across the geometry, identifying areas of elongation and compression, which is vital for detecting regions susceptible to deformation. Finally, stress concentration zones were pinpointed to locate critical areas of peak stress, essential for optimizing the design to prevent failure and improve performance. This comprehensive assessment framework ensures a robust analysis of nose geometries, providing data critical to guiding further design optimizations and improvements under dynamic reentry conditions.

6 Validation and Reliability

The accuracy of the results was validated by comparing the deformation and stress distributions obtained from the simulations with theoretical calculations and experimental data reported in previous studies [20]. This comparison confirmed the reliability of the computational approach and ensured consistency with established benchmarks. Additionally, a mesh convergence analysis was conducted to evaluate the numerical robustness of the simulations [2]. By systematically refining the mesh and monitoring the variation in results, it was verified that the solution was independent of mesh size. This step was crucial in eliminating numerical errors and enhancing the precision of the analysis. These validation techniques strengthened the study's credibility, providing confidence in the findings' accuracy and applicability to real-world scenarios.

7 Results and Discussion

The study evaluates the structural performance of aeroshells with flat, hemispherical, and pointed nose configurations under atmospheric re-entry conditions. The comparative analysis focuses on total deformation, equivalent stress, and equivalent strain across three materials: structural steel, aluminum alloy, and epoxy carbon woven prepreg. The results in Tables 2-4 present the following key observations.

7.1 Total Deformation

The flat nose design demonstrates the highest total deformation across all materials, indicating reduced structural rigidity under re-entry stresses. epoxy carbon woven recorded the highest deformation, with a maximum of 14.57 m, followed by aluminum alloy at 6.1225 m and structural steel at 2.24130 m. This indicates that the flat nose is less able to maintain structural integrity under extreme loading. In contrast, the hemispherical nose exhibited lower total deformation, showcasing superior structural stability. Maximum values for the hemispherical nose were 5.90930 m for epoxy carbon woven, 2.08880 m for Aluminum Alloy, and 0.76051 m for structural steel. The pointed nose configuration displayed the lowest deformation levels, with maximum values of 0.00235 m for epoxy carbon woven, 0.00646 m for aluminum alloy, and 0.99946 m for Structural Steel. This suggests that the pointed nose balances flexibility and rigidity, making it structurally more stable than the flat nose but slightly less rigid than the hemispherical nose.

7.2 Equivalent Stress

The flat nose generates the highest equivalent stress among all configurations, with epoxy carbon woven reaching a peak stress of 2.50 × 10^10 Pa, followed by aluminum alloy (1.65 × 10^10 Pa) and structural steel (1.68 × 10^10 Pa). This high-stress concentration indicates that the flat nose is more susceptible to material failure during re-entry. The hemispherical nose design exhibits the lowest stress levels, emphasizing its ability to distribute aerodynamic and thermal loads more effectively. Maximum stress values for the hemispherical nose were 4.14×10^{10} Pa for epoxy carbon woven, 2.75×10^{10} Pa for aluminum alloy, and 2.74×10^{10} Pa for structural steel. The pointed nose produced slightly higher stresses than the hemispherical configuration but remained considerably lower than the flat nose. Maximum stress values for the pointed nose were 8.21×10^{8} Pa for epoxy carbon woven, 9.01×10^{8} Pa for aluminum alloy, and 9.05×10^{8} Pa for structural steel. This highlights its ability to mitigate stresses while maintaining structural efficiency.

7.3 Equivalent Strain

The flat nose also recorded the highest strain levels, with epoxy carbon woven at 1.49030 m/m, aluminum alloy at 0.23368 m/m, and structural steel at 0.08422 m/m. These values signify significant deformation under high-temperature and aerodynamic loads, possibly leading to instability during re-entry. The hemispherical nose demonstrated the lowest strain values, with Epoxy carbon woven at 0.99946 m/m, aluminum alloy at 0.38994 m/m, and structural steel at 0.13775 m/m, making it the most stable design in terms of strain resistance. The pointed nose showed intermediate strain values, with epoxy carbon woven at 0.12709 m/m, aluminum alloy at 0.01272 m/m, and structural steel at 0.00453 m/m, establishing its balanced performance between rigidity and adaptability.

7.4 Material Comparison:

Among the materials, epoxy carbon woven consistently recorded the highest deformation and strain values across all configurations, reflecting its flexibility and high energy-absorption capacity. However, its high-stress resistance makes it suitable for applications that require lightweight, impact-absorbing materials. Structural steel exhibited the lowest deformation and strain values, indicating superior rigidity and load-bearing capacity. Aluminum alloy emerged as a middle-ground material, balancing lightweight properties with moderate deformation and stress resistance, making it versatile for aerospace applications. The hemispherical nose design is the most structurally efficient configuration, demonstrating significantly minimized deformation, stress, and strain under extreme atmospheric re-entry conditions. This superior performance makes it ideal for aerospace applications that demand high stability, durability, and reliable load distribution during re-entry. On the other hand, the pointed nose provides a balanced compromise between rigidity and flexibility, making it suitable for scenarios where moderate structural efficiency is acceptable. In contrast, despite its straightforward design, the flat nose exhibits substantial limitations due to higher deformation, stress, and strain levels, which could compromise its structural integrity during critical re-entry phases. These findings offer valuable insights into optimizing aeroshell designs and selecting suitable materials, ensuring enhanced safety, reliability, and structural efficiency in challenging aerospace environments.

Table 2: Deformation, Stress, and Strain Analysis in Flat Nose Geometry

FLAT NOSE		
Total Deformation (m)		
	Maximum	Average
Structural Steel	2.24130	0.04180
Aluminum Alloy	6.12250	0.11210
Epoxy Carbon Woven (395 Gpa) Prepeg	14.57000	0.32096
Equivalent Stress (Pa)		
	Maximum	Average
Structural Steel	1.68E+10	7.53E+08
Aluminum Alloy	1.65E+10	7.43E+08
Epoxy Carbon Woven (395 Gpa) Prepeg	2.50E+10	7.85E+08
Equivalent Strain (m/m)		
	Maximum	Average
Structural Steel	0.08422	0.00534
Aluminum Alloy	0.23368	0.01481
Epoxy Carbon Woven (395 Gpa) Prepeg	1.49030	0.07016

Table 3: Deformation, Stress, and Strain Analysis in Hemispherical Nose Geometry

HEMISPHERICAL NOSE		
Total Deformation (m)		
	Maximum	Average
Structural Steel	0.76051	0.00876
Aluminum Alloy	2.08880	0.02411
Epoxy Carbon Woven (395 Gpa) Prepeg	5.90930	0.12319
Equivalent Stress (Pa)		
	Maximum	Average
Structural Steel	2.74E+10	8.21E+08
Aluminum Alloy	2.75E+10	8.16E+08
Epoxy Carbon Woven (395 Gpa) Prepeg	4.14E+10	8.76E+08
Equivalent Strain (m/m)		
	Maximum	Average
Structural Steel	0.13775	0.00486
Aluminum Alloy	0.38994	0.01354
Epoxy Carbon Woven (395 Gpa) Prepeg	0.99946	0.08122

Table 4: Deformation, Stress, and Strain Analysis in Pointed Nose Geometry

POINTED NOSE		
Total Deformation (m)		
	Maximum	Average
Structural Steel	0.00235	0.00160
Aluminum Alloy	0.00646	0.00432
Epoxy Carbon Woven (395 Gpa) Prepeg	0.05697	0.03286
Equivalent Stress (Pa)		
	Maximum	Average
Structural Steel	9.05E+08	1.30E+08
Aluminum Alloy	9.01E+08	1.30E+08
Epoxy Carbon Woven (395 Gpa) Prepeg	8.21E+08	1.32E+08
Equivalent Strain (m/m)		
	Maximum	Average
Structural Steel	0.00453	0.00069
Aluminum Alloy	0.01272	0.00194
Epoxy Carbon Woven (395 Gpa) Prepeg	0.12709	0.01882

8 Conclusion

This study analyzed the structural performance of aeroshells with flat, hemispherical, and pointed nose configurations under atmospheric re-entry conditions. The investigation focused on critical parameters such as total deformation, equivalent stress, and equivalent strain across three distinct materials: structural steel, aluminum alloy, and epoxy carbon woven prepreg. The results highlighted significant variations in aerodynamic efficiency and structural robustness across nose geometries and material selections. The hemispherical nose configuration emerged as the most structurally efficient design, demonstrating superior performance with minimal deformation, stress, and strain across all materials. Its ability to effectively distribute aerodynamic and thermal loads enhances its stability and durability, making it the most suitable choice for high-demand re-entry applications requiring exceptional structural integrity. The pointed-nose configuration offered balanced performance, combining moderate rigidity with sufficient energy absorption. In contrast, the flat nose design exhibited the highest deformation, stress, and strain values, indicating substantial limitations in structural stability under extreme re-entry conditions, making it the least viable option. Among the materials studied, epoxy-carbon woven exhibited remarkable stress resistance and excellent energy absorption. However, its higher deformation and strain values suggest it is better suited to applications that prioritize lightweight structures and flexibility. Structural steel demonstrated the lowest deformation and strain, reflecting its high rigidity and superior load-bearing capacity, though its higher density may limit its application where weight is critical. Aluminum alloy, on the other hand, presented a practical compromise, combining moderate strength with lightweight properties, making it a versatile material for various aerospace applications. In conclusion, the hemispherical nose configuration, coupled with advanced materials such as epoxy-carbon woven fabric or aluminum alloy, provides an optimal solution for aeroshells subjected to extreme re-entry environments. This study underscores the importance of tailoring nose geometry and material selection to enhance the aerodynamic and structural performance of re-entry vehicles. By leveraging the strengths of innovative materials and efficient designs, this research provides valuable insights for developing safer, more reliable aerospace systems, paving the way for advancements in future atmospheric re-entry applications.

References

1 Allen, H. J., & Eggers, A. J. (1957). A study of the motion and aerodynamics of a blunt body in a hypersonic flow. *NACA Technical Report, 1381,* 1–36.
2 Knacke, T. W. (1991). *Design of aerodynamic decelerators.* American Institute of Aeronautics and Astronautics (AIAA).
3 Braun, R. D., & Manning, R. M. (2007). Mars exploration entry, descent, and landing challenges. *Journal of Spacecraft and Rockets, 44*(2), 310–323.
4 Heppenheimer, T. A. (2006). *Facing the heat barrier: A history of hypersonics.* NASA SP-4232. NASA
5 Anderson, J. D. (2016). *Fundamentals of aerodynamics* (6th ed.). McGraw-Hill.
6 Davis, M. E. (2019). *Hypersonic and high-temperature gas dynamics* (3rd ed.). AIAA.
7 Bond, E. J. (2020). A comparison of aeroshell designs for Mars entry systems. *International Conference on Aerospace and Mechanical Engineering, 12*(3), 456–463
8 Schetz, J. A. (2022). *Aerodynamics of high-speed trains, vehicles, and spacecraft.* Cambridge University Press.
9 Singh, M. K. (2019). Numerical modeling of drag coefficients for blunt-body reentry vehicles. *International Journal of Aerodynamics, 15*(3), 87–101.
10 ANSYS. (2023). Best practices for structural and thermal analysis of aerospace components. *ANSYS Workbench Documentation.*
11 Blanchard, C., & Austin, M. (2021). Finite element analysis in aerospace structural engineering. *AIAA Journal, 58*(7), 1423–1436.
12 Ahmed, K., & Sharma, N. (2020). Thermal protection and aerodynamic design of reentry vehicles. *Aerospace Research Journal, 33*(4), 199–210.

13 Srivastava, V., et al. (2023). Materials for hypersonic reentry vehicles: A comprehensive review. *Materials Science and Engineering, 23,* 321–343.
14 Yoshida, H., & Matsuo, T. (2022). Strain analysis and stress distribution in composite materials for aerospace applications. *Composite Structures Journal, 98,* 120–129.
15 Park, G. A. (2021). *Introduction to space vehicle design and analysis* (2nd ed.). Springer.
16 He, B., Sun, H., & Zhang, T. (2021). Optimization of reentry vehicle nose shapes using computational fluid dynamics. *Computational Mechanics in Aerospace Engineering, 47*(2), 209–222.
17 NASA. (n.d.). Entry, descent, and landing systems. *NASA Engineering Design Handbook.* Retrieved from https://www.nasa.gov
18 Karman, T. (2020). Aerodynamic heating and reentry physics. *Journal of Spacecraft and Rockets, 45*(2), 123–134.
19 NASA. (2021, October). *NASA's 2020 planetary science research: Overview and highlights* (NP-2020-02-2805-HQ). https://www.nasa.gov/wp-content/uploads/2021/10/np-2020-02-2805-hq.pdf
20 Padhye, R. P., & Joshi, S. C. (2023). CFD analysis of drag coefficient and heat transfer for blunt body configurations. *Journal of Thermophysics and Heat Transfer, 36*(1), 102–110.
21 Ali, A. (2023). Finite element modeling techniques for aerospace applications. *Advances in Structural Engineering, 29*(5), 1204–1217